ISSN 2706-655X Vol.3, Issue 3: 28-35, DOI: 10.25236/IJFET.2021.030305

# Optimal design of sensor structure based on virtual calibration test

**Yong Wei*, Juncheng Lv, Yonghui Jia**

*SAIC GM Wuling Automobile Co., Ltd., No.18 Hexi Road, Liunan District, Liuzhou, Guangxi Zhuang Autonomous Region, 545007, China*
**Corresponding author: yong.wei@sgmw.com.cn*

***Abstract:*** *The design of wheel six-component force sensor includes elastic body, strain gauges distribution scheme, signal acquisition and processing and so on. In this paper, the virtual calibration test is used to optimize the structure of the sensor elastic body. According to the structure and principle of the self-developed six component force sensor calibration test-bed, a set of calibration device is designed for the sensor. The stress distribution and strain output of the elastic body are obtained by finite element method. The optimization of elastic body is carried out from the requirements of material strength and coupling rate of output signal. Finally, the sensor elastic body structure which meets the strength requirements and has low coupling rate is obtained.*

***Keywords:*** *wheel six-component force sensor; structure optimization; virtual calibration test; finite element method*

## 1. Introduction

The wheel six component force sensor is used to measure the longitudinal force Fx, lateral force Fy, vertical force Fz, heeling moment Mx, twist torque My and aligning torque Mz. These forces and torques are of great significance for vehicle road test [1-3]. Therefore, sensors are widely used in the process of automobile design and development, and play an important role.

The structure design of the sensor elastic body mainly considers two aspects: one is that the structure meets the strength requirements; the other is that the coupling rates between all channels are as small as possible. Due to the complex structure of elastic body, it is difficult to verify the above two points by theoretical calculation method. However, it is very fast and effective to calculate them by using finite element method [4]. The virtual calibration test with ABAQUS software can obtain the stress distribution nephogram of the sensor, so as to judge whether the elastic body meets the strength requirements. Select the nodes where the strain gauge are pasted and set them as node sets. Then the strain of the node sets can be calculated to obtain the coupling rates between all channels.

The remainder of this paper is organized as follows. In the second section, the principle and method of calibration test are introduced. The connection method of the sensor and its adapters and the transmission path of the force are briefly described. In the third section, the mesh size selection, constraint setting and strain calculation method of virtual calibration test are introduced. In the fourth section, the simulation results of stress and strain are given. The sensor is optimized from two aspects of structural strength and coupling rate. The fifth section is the conclusion of this paper.

## 2. Experiment

### *2.1 Calibration principle*

Resistance strain gauge measurement and piezoelectric effect measurement are two common measurement methods of wheel sensor. Resistance strain measurement is widely used because of its general applicability [5-6]. The measurement principle of a strain-gauge-based sensor lies in the two principles of material mechanics, one is linear relationship between structural strain and external load, the other one is superposition principle [7]. Strain gauges make up Wheatstone bridge. When the sensor is stressed, the elastic body deformation causes the change of strain gauge resistance. Then the output voltage of Wheatstone bridge changes. The purpose of calibration test is to obtain the relationship

ISSN 2706-655X Vol.3, Issue 3: 28-35, DOI: 10.25236/IJFET.2021.030305

between the force or torque and the outputs of the sensor [8]. When an ideal sensor inputs force or torque in one direction, only the corresponding bridge voltage changes. However, due to the processing of the elastic body and the location of the strain gauges, the measurement channels interact and couple with each other. Through the calibration test, the decoupling matrix can be obtained, which can be used to calculate more accurate wheel forces.

The relationship between applied load F(Fx,Fy,Fz,Mx,My,Mz) and output voltage U(UFx ,UFy ,UFz ,UMx ,UMy ,UMz ) is

$$U=CF \tag{1}$$

Where the matrix C is a 6×6 compliance matrix whose elements Cij represents the strain contribution at bridge circuit i due to a unit pure load j [9].

There is a linear relationship between the load F and the output voltage U of the sensor. By applying the force Fx alone, the first column $C_{i1}$ in the matrix C can be obtained. Similarly, if Fy, Fz, Mx, My, Mz are applied separately in turn, other elements of matrix C can be obtained. Furthermore, the decoupling matrix $C^{-1}$ can be calculated by matrix C. In the end, the actual forces of the wheel during road test can be calculated according to $F=C^{-1}U$.

### *2.2 Calibration method*

The self-developed six component force calibration test-bed of the sensor is shown in Fig. 1 and Fig. 2. The calibration test-bed is composed of hydraulic cylinder, standard single component force sensor, support arm, bearing seat, support base, etc. By changing the direction of the hydraulic oil, the hydraulic cylinder can realize two loading directions: push and pull. The hydraulic cylinder is connected with the support arm, which can rotate around the bearing seat to realize the horizontal and vertical loading. Through the combination of hydraulic cylinder and adapters in different positions, the calibration test-bed can realize the independent loading in six directions.

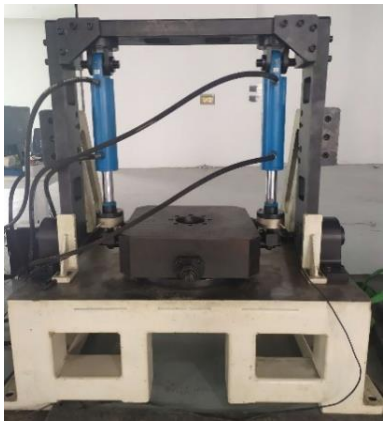

*Figure 1: Vertical hydraulic cylinder*

*Figure 2: Horizontal hydraulic cylinder*

Fig. 3 shows the sensor and its adapters. From top to bottom are iron cap, sensor, inner ring adapter, outer ring adapter and fixed plate. The iron cap is connected with the hydraulic cylinder for loading and acts as a tire. The fixed plate is connected with the support base and acts as the automobile body. The sensor is composed of inner ring, outer ring and strain beam, in which the inner ring is the loading end and the outer ring is the fixed end. The specific connection relationship is shown in Fig. 4. The forces transmission path is: iron cap→inner ring adapter→sensor→outer ring adapter→fixed plate.

ISSN 2706-655X Vol.3, Issue 3: 28-35, DOI: 10.25236/IJFET.2021.030305

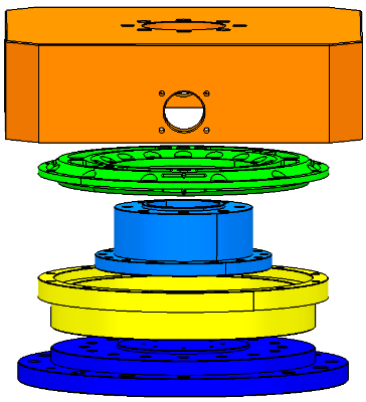

*Figure 3: The sensor and its adapters*

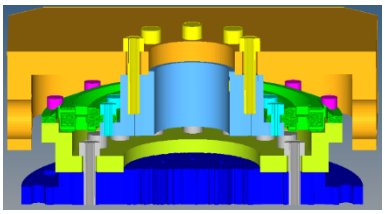

*Figure 4: Connection relationship*

## 3. Virtual calibration test

After the initial shape of the sensor elastic body is determined, we use the finite element analysis method to optimize the structure. In the finite element simulation analysis, the more the number of elements, the longer the calculation time. For the purpose of improving the calculation efficiency, the calibration system model is simplified. Only the sensor and its adapters are selected for simulation analysis, and the other parts are replaced by constraint conditions.

### *3.1 Meshing*

Different sizes of meshes are used to divide the assembly according to different analysis requirements. Small meshes are used in the position of strain beam. Therefore, more accurate strain information can be obtained. The connecting bolts use medium meshes, which can better connect different parts. The other parts use large meshes, which can simplify the analysis process and improve the calculation speed.

According to the properties of general steel, the modulus of elasticity is set at 206 GPa and Poisson's ratio is 0.3. Assemble all the components and the cross section of the assembly is shown in Fig. 5.

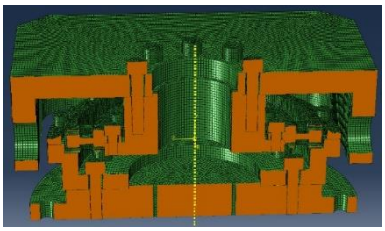

*Figure 5: Cross section of the assembly*

### *3.2 Constraints*

As shown in Fig.6, the bottom surface of the fixed plate is coupled with its center point through coupling constraint, which can limit the six degrees of freedom of the fixed plate to remain stationary. Four nodes are set around the iron cap, which are located at the loading center of the hydraulic cylinder, as shown in Fig.7. They are coupled with the iron cap. The load of hydraulic cylinder is simulated by applying different forces in different directions and sizes through these nodes.

ISSN 2706-655X Vol.3, Issue 3: 28-35, DOI: 10.25236/IJFET.2021.030305

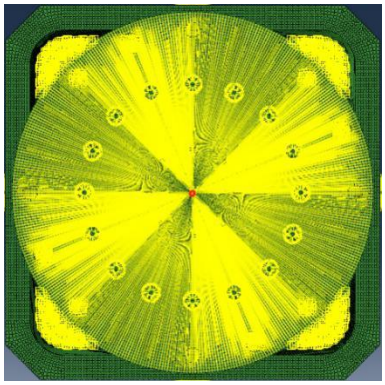

*Figure 6: Coupling constraint of the fixed plate*

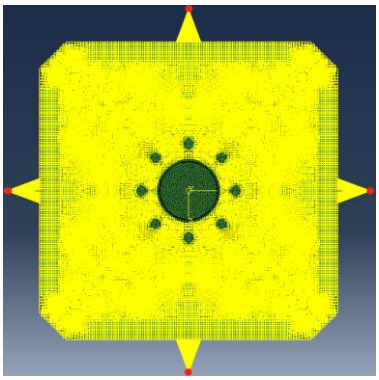

*Figure 7: Coupling constraint of the iron cap*

The components of the assembly are connected by bolts, and the corresponding simulation settings is shown in Fig.8. Set element sets for bolt face and corresponding hole face, and paste them together with tie command, as shown in the red mesh area. Set a section at the bolt rod, and apply the preload at the section position, as shown by the yellow arrow in fig.8. Through the above method, actual bolt connection of the assembly can be simulated.

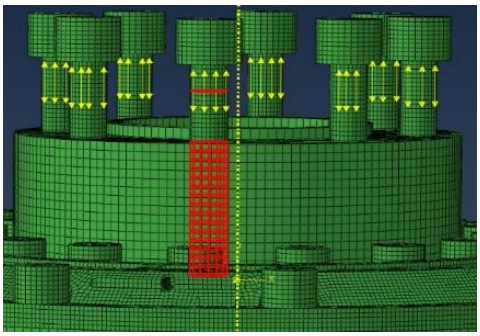

*Figure 8: Bolted connection*

### *3.3 Result output and calculation*

Each strain gauge is simulated by three collinear and equidistant points. The position of the points are at the pasted position on the beam of the strain gauges, as shown in Fig.9. The strain of each strain gauge can be calculated by outputting the initial coordinates of the node sets corresponding to all strain gauges and the coordinates after loading and deformation. All strain gauges of this sensor are attached to four beams, as shown in Fig.10.

ISSN 2706-655X Vol.3, Issue 3: 28-35, DOI: 10.25236/IJFET.2021.030305

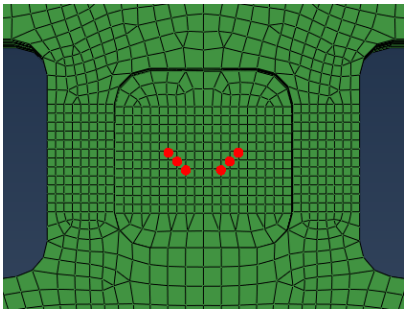

*Figure 9: Strain gauge simulation method*

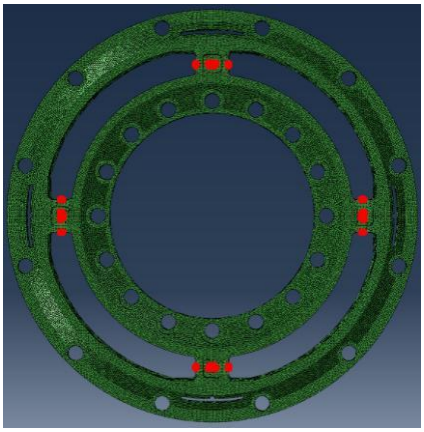

*Figure 10: All strain gauges of the sensor*

The output of virtual calibration test is strain value, while the output of actual test is voltage. In order to compare the differences between them, it is necessary to convert the strain into voltage. The strain gauges are connected by Wheatstone bridge, as shown in Fig.11.

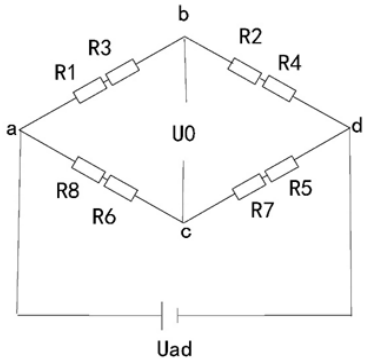


*Figure 11: Wheatstone bridge*

The relationship between strain and output voltage is

$$U_0 = \frac{k}{8}(\varepsilon 1 + \varepsilon 3 + \varepsilon 5 + \varepsilon 7 - \varepsilon 2 - \varepsilon 4 - \varepsilon 6 - \varepsilon 8)U_{ad} \quad (2)$$

Where k is the sensitivity coefficient of strain gauge, ε1- ε8 is the strain output of strain gauge R1-R8, and $U_{ad}$ is the strain output of strain gauge R1-R8. $U_{ad}$ is the supply voltage and $U_0$ is the output voltage.

## 4. Results and discussion

The virtual calibration test can obtain some data information such as the stress and strain of the sensor, which can be used to optimize the structure of the sensor. It mainly adopts the method of finite element analysis, which has high calculation efficiency and high precision.

Taking the calibration test in Mx direction as an example, the sensor is loaded at full scale, and then

ISSN 2706-655X Vol.3, Issue 3: 28-35, DOI: 10.25236/IJFET.2021.030305

the stress distribution diagram of the elastic body of the sensor can be obtained, as shown in Fig.12. The stress distribution diagram shows the stress state of the structure, from which we can find the location of the maximum stress, that is, the dangerous point. Therefore, the structure can be optimized according to the simulation results. The size and shape of dangerous points should be adjusted properly to reduce the maximum stress and meet the strength requirements.

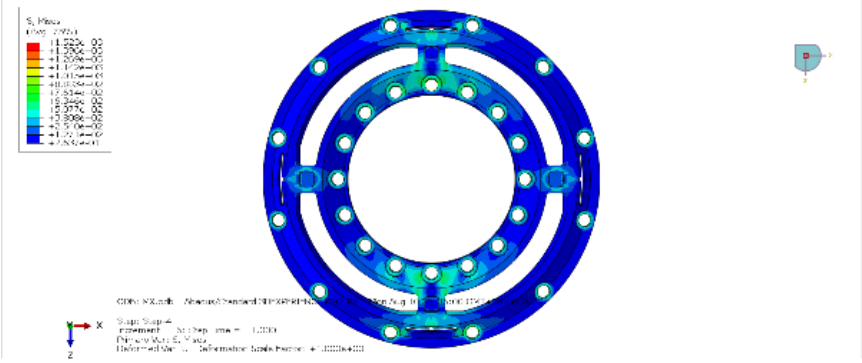

*Figure 12: The stress distribution diagram under Mx loading*

There will be interference between each measurement channel of the sensor, and its magnitude is expressed by the coupling rate. The coupling rate formula is expressed as

$$e_{ij} = \frac{u_{ij}}{u_{ii}} \tag{3}$$

where $u_{ij}$ is the output signal generated by Wheatstone bridge designed for load component i when load component j acts alone, $u_{ii}$ is the output signal generated by Wheatstone bridge designed for load component i when load component i is applied separately.

According to equation (2), the output voltage $u$ is directly proportional to the average strain ε, so the coupling rate can be calculated according to the strain of simulation results. Then, analyze the possible reasons of large coupling in the results, and optimize the structure of the sensor. The average strain output of the optimized structure is shown in Table 1, and the corresponding coupling rate is shown in Table 2.

*Table 1: Average strain of six components*

| **ε** | **Strain output(×10-6mm/mm)** | | | | | |
|---|---|---|---|---|---|---|
| | **Fx** | **Fy** | **Fz** | **Mx** | **My** | **Mz** |
| εFx | 364.88 | -0.06 | -0.18 | 0.12 | -0.07 | -2.91 |
| εFy | 3.27 | 321.12 | 3.22 | 3.93 | 3.51 | 3.94 |
| εFz | 0.07 | -0.02 | 364.97 | 2.69 | -0.02 | 0.49 |
| εMx | -0.01 | 0.004 | 2.6 | 1235.42 | 0.02 | -0.01 |
| εMy | 0.01 | 0.03 | 0.01 | 0.04 | 730.98 | 0.05 |
| εMz | -2.6 | 0.01 | 0.001 | 0.02 | 0.01 | 1235.46 |

*Table 2: Coupling rate of six components*

| **e** | **Coupling rate (%)** | | | | | |
|---|---|---|---|---|---|---|
| | **Fx** | **Fy** | **Fz** | **Mx** | **My** | **Mz** |
| eFx | - | -0.02 | -0.05 | 0.03 | -0.02 | -0.8 |
| eFy | 1.02 | - | 1 | 1.22 | 1.09 | 1.23 |
| eFz | 0.02 | -0.004 | - | 0.74 | -0.01 | 0.13 |
| eMx | -0.001 | 0.0003 | 0.21 | - | 0.001 | -0.001 |
| eMy | 0.002 | 0.004 | 0.002 | 0.01 | - | 0.01 |
| eMz | -0.21 | 0.0004 | 0.001 | 0.002 | 0.001 | - |

Through the virtual calibration test, the coupling rate between all channels is reduced to less than 1.5%, so the optimization results meet the requirements of application. After structure optimization, the sensor entity is processed as shown in Fig. 13.

ISSN 2706-655X Vol.3, Issue 3: 28-35, DOI: 10.25236/IJFET.2021.030305

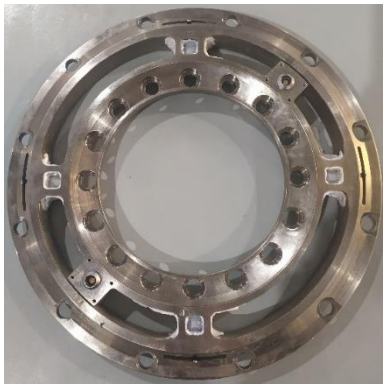

*Figure 13: Wheel six-component force sensor*

## 5. Conclusions

In this paper, the virtual calibration test method is used to optimize the structure of the wheel six-component force sensor. The virtual calibration test uses commercial finite element software ABAQUS, which has high calculation efficiency and accuracy. According to the simulation results, the structure is optimized from two aspects of strength and coupling rate. First of all, find out all the large stress position, modify its size and shape, etc., to reduce the maximum stress. Repeat the optimization several times until all positions meet the strength requirements. After that, calculate the coupling rates between each two channels. Analyze the reason of high coupling rate according to the simulation results, and then adjust the structure. Through the virtual calibration test, the structure whose strength meets the design requirements and the coupling rate is less than 1.3% is obtained.

In the future work, the sensors processed according to the optimized results will be calibrated. In addition, the sensor will be verified by bench test with a standard sensor product.

**Author Contributions:** Conceptualization, Tao Liu and Yanru Suo; methodology, Yong Wei; software, Chunying Jin; validation, Yong Wei; formal analysis, Tao Liu and Chunying Jin; investigation, Yanru Suo; resources, Yong Wei; data curation, Tao Liu and Yanru Suo; writing—original draft preparation, Tao Liu; writing—review and editing, Yanru Suo; visualization, Chunying Jin.; supervision, Yong Wei; project administration, Yong Wei; funding acquisition, Yanru Suo. All authors have read and agreed to the published version of the manuscript.

**Funding:** This research was funded by Liuzhou Science and Technology Project, grant number 2018AA20501.

**Conflicts of Interest:** The authors declare no conflict of interest.

## Acknowledgements

This work was supported by Liuzhou Science and Technology Project [NO. 2018AA20501].

## References

*[1] Corno M, Gerard M, Verhaegen M, Holweg E. Hybrid ABS control using force measurement. IEEE Trans Control Syst. 2012; 20: 1223–1235. doi: 10.1109/TCST.2011.2163717.*
*[2] Pavkovic D, Deur J, Hrovat D, Burgio G. A switching traction control strategy based on tire force feedback. IEEE conference on control applications and intelligent control, Saint Petersburg, Russia, 2009; 8–10: 588–593. doi: 10.1109/CCA.2009.5281121.*
*[3] Liu QH and Zhang WG. Design of acquisition system for road loading spectra data based on wheel force transducer. Jiangsu Univ (Nat Sci Edition) 2011; 32(4): 389–393.*
*[4] Lihang Feng, Guoyu Lin, Weigong Zhang, Dong Dai. Inertia Coupling Analysis of a Self-Decoupled Wheel Force Transducer under Multi-Axis Acceleration Fields. PLOS ONE, 2015, 10(2). doi: 10.1371/journal.pone.0118249.*
*[5] Weiblen W and Hofmann T. Evaluation of different designs of wheel force transducers. SAE paper 980262, 1998.*

ISSN 2706-655X Vol.3, Issue 3: 28-35, DOI: 10.25236/IJFET.2021.030305

*[6] Weiblen W, Kockelmann H and Burkard H. Evaluation of different designs of wheel force transducers (part II).SAE paper 1999-01-1037, 1999.*
*[7] Xiang Li, Hui He, Hongqiang Ma. Structure design of six-component strain-gauge-based transducer for minimum cross-interference via hybrid optimization methods. Structural and Multidisciplinary Optimization, 2019, 60(1).*
*[8] Guoyu Lin, Han Pang, Weigong Zhang, Dong Wang, Lihang Feng. A self-decoupled three-axis force sensor for measuring the wheel force. Proceedings of the Institution of Mechanical Engineers, 2014, 228(3).*
*[9] Lihang Feng, Guoyu Lin, Weigong Zhang, Han Pang, Tie Wang. Design and optimization of a self-decoupled six-axis wheel force transducer for a heavy truck. Proceedings of the Institution of Mechanical Engineers, Part D: Journal of Automobile Engineering, 2015, 229(12). doi:10.1177/0954407014566439.*